ACS Energy LETTERS

http://pubs.acs.org/journal/aelccp

Bright Lead-Free Inorganic $CsSnBr_3$ Perovskite Light-Emitting Diodes

Jung-Min Heo,[#] Himchan Cho,[#] Seong-Chul Lee, Min-Ho Park, Joo Sung Kim, Hobeom Kim, Jinwoo Park, Young-Hoon Kim, Hyung Joong Yun, Eojin Yoon, Dong-Hyeok Kim, Soyeong Ahn, Sung-Joo Kwon, Chan-Yul Park, and Tae-Woo Lee*

Cite This: *ACS Energy Lett.* 2022, 7, 2807−2815

Read Online

ACCESS | Metrics & More | Article Recommendations | Supporting Information

ABSTRACT: **Tin-based perovskites have emerged as lead-free alternatives, but their application in perovskite light-emitting diodes (PeLEDs) has been limited due to the low chemical stability and inhomogeneity of the inorganic $CsSnBr_3$ films using solution processing. Here, we demonstrate bright (~160 cd m^{-2}) $CsSnBr_3$ PeLEDs made by introducing co-additives consisting of SnF_2 and a grain-growth inhibitor (1,3,5-tris(*N*-phenylbenzimidazol-2-yl)benzene). The use of co-additives increased the number of nucleation sites during the crystallization process of $CsSnBr_3$, and consequently yielded uniform $CsSnBr_3$ films with decreased grain size and improved defect passivation. The crystallization-controlled $CsSnBr_3$ PeLEDs had a maximum luminance of ~160 cd m^{-2}, i.e., ~7500 times brighter than that of the control devices (without additive, 0.02 cd m^{-2}), and a long device lifetime of ~30 h at 58 cd m^{-2}. Our work suggests that control of the crystallization of $CsSnBr_3$ during film formation is an important requirement to increase the luminescence efficiency and stability of tin-based PeLEDs.**

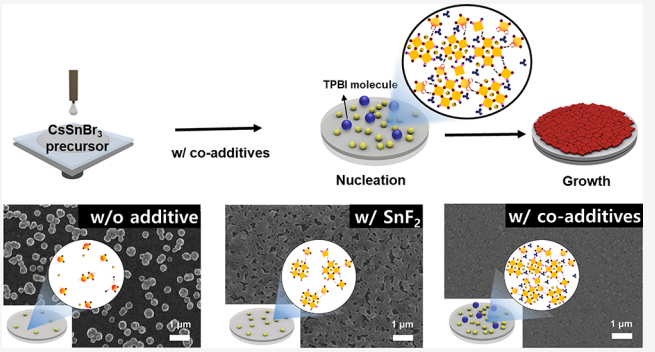

Metal halide perovskites (MHPs) are regarded as promising light-emitting materials for light-emitting diodes (LEDs) and displays due to several inherent traits: (i) superior color purity (full width at half-maximum (fwhm) ~20 nm), (ii) easy tuning of emission wavelength, (iii) solution processability, (iv) high charge-carrier mobility, and (v) energy levels comparable with those of most organic semiconductors.[1−4] The early-stage perovskite light-emitting diodes (PeLEDs) used 3D polycrystalline MHPs, which have advantages of simplicity in the preparation of precursor solutions and in the thin-film formation process.[4−9] Subsequently, the electroluminescence (EL) characteristics of PeLEDs were significantly improved by various approaches, such as solvent treatments to control the size of the perovskite grains,[5,7] use of additives to passivate defects,[5,10−12] and synthesis of colloidal perovskite nanocrystals.[13,14]

However, most existing PeLEDs use lead-based perovskites, and the toxicity of lead is a huge obstacle for industrialization. The toxicity of Pb violates the "directive on the Restriction of the use of Hazardous Substances (RoHS) in electrical and electronic equipment",[15] which is a treaty to avoid using harmful materials. For this reason, many researchers have studied lead-free perovskite materials.[16−23] Sn is considered as the most promising alternative to Pb due to its similarity in chemical characteristics (e.g., oxidation state and ionic radius), so this element has been widely used for perovskite solar cells.[24,25] However, Sn-based MHPs are chemically very unstable because of self-oxidation of Sn^{2+} to Sn^{4+}, which acts as a *p*-type dopant in MHPs; this self-doping process increases the hole concentration and thereby alters the MHP's electronic properties from semiconducting to metallic.[17] Also, the self-oxidation of Sn^{2+} to Sn^{4+} leads to the formation of Sn vacancies in Sn-based MHP polycrystalline films. Because of this fundamental problem, only a few studies have reported lead-free Sn-based PeLEDs. Visible-light-emitting lead-free PeLEDs have been achieved using low-dimensional organic−inorganic hybrid MHPs, such as $(PEA)_2SnI_xBr_{4-x}$; however, the luminance (L = 0.15 cd m^{-2}) and current efficiency (CE = 0.029 cd A^{-1}) were limited.[26] Recently, lead-free PeLEDs were reported with high color purity, obtained using the same low-dimensional MHP

Received: April 29, 2022
Accepted: June 7, 2022
Published: August 3, 2022

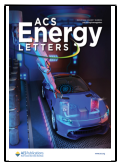

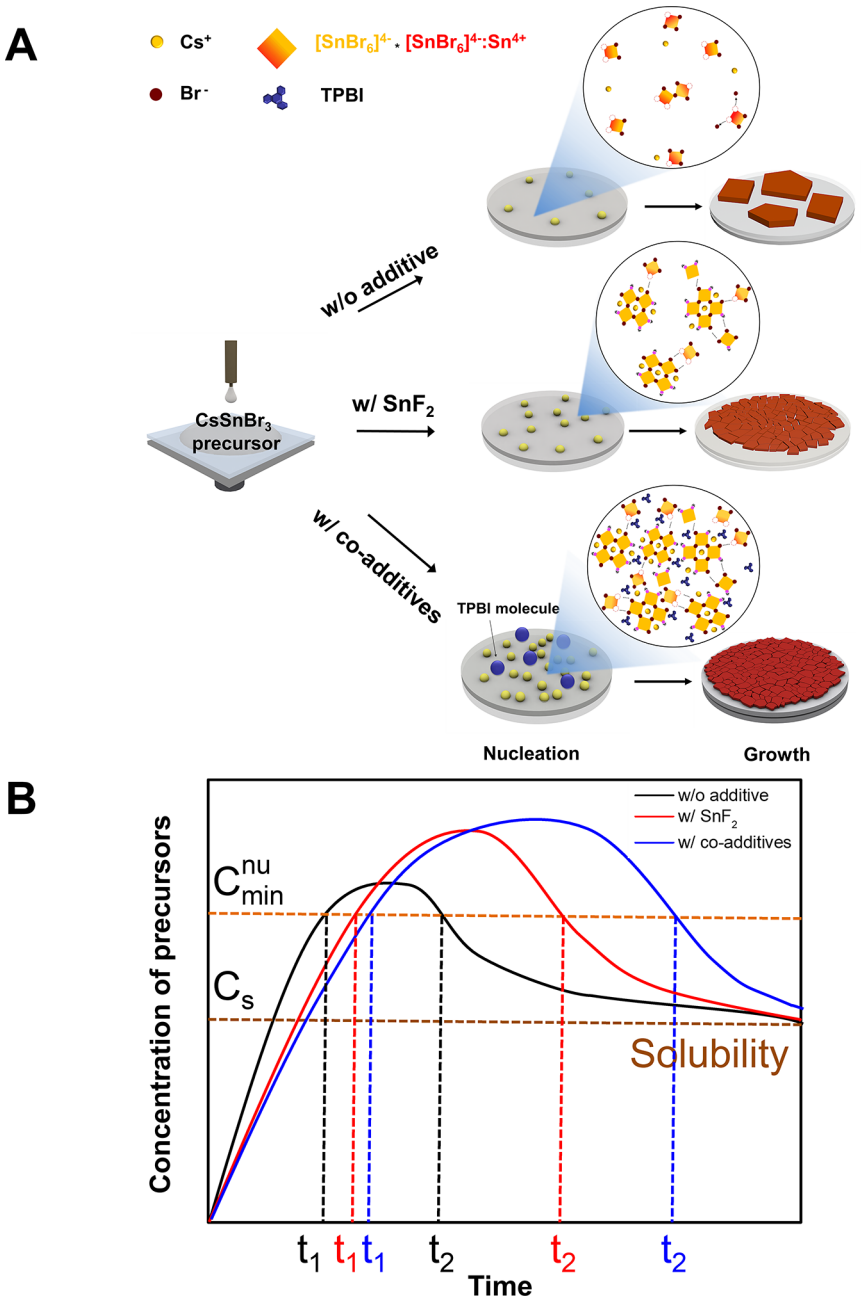

Figure 1. (A) Schematic illustration of the crystallization process of $CsSnBr_3$ with additive engineering. (B) Modified LaMer diagram for the $CsSnBr_3$ crystallization process with additive engineering strategy.

(PEA_2SnI_4).[27] The researchers suppressed the oxidation of Sn^{2+} by using H_3PO_2 as an additive, but their lead-free PeLEDs still showed low brightness (L = 70 cd m^{-2}). Although there has recently been great progress in all-inorganic solution-processed $CsSnI_3$ infrared PeLEDs,[28,29] visible light lead-free PeLEDs still need further development for display applications.

Inorganic $CsSnBr_3$ has a higher thermal stability (thermal decomposition temperature of 437 °C) than organic/inorganic hybrid Sn-based MHPs.[30] Therefore, $CsSnBr_3$ can be more compatible with high-temperature processing and more resistant to Joule heating in PeLEDs. However, the formation of uniform $CsSnBr_3$ polycrystalline films by solution processing is difficult due to the spontaneous formation of Sn vacancies between $CsSnBr_3$ grains by self-oxidation of Sn^{2+} to Sn^{4+};[23] the non-uniformity results in poor EL characteristics in PeLEDs.[28,31] To overcome this problem, SnF_2 has been used as an additive for Sn-based perovskite optoelectronic devices.[20,32−34] However, excessive addition of SnF_2 often leads to various problems, such as phase segregation in MHP films, formation of nanoplatelet-like structures, and poor device performance.[17,35] Therefore, it is essential to find an effective strategy to fabricate uniform Sn-based MHPs polycrystalline films that have high packing density, while suppressing the self-oxidation process.

Here, we present a simple way to control the crystallization process of solution-processed perovskites films for fabricating uniform $CsSnBr_3$ polycrystalline films and bright lead-free PeLEDs. We introduced an organic/inorganic co-additive composed of SnF_2 and 1,3,5-tris(*N*-phenylbenzimidazol-2-yl)-benzene (TPBI). SnF_2 functions as a reducing agent (or an

https://doi.org/10.1021/acsenergylett.2c01010
ACS Energy Lett. 2022, 7, 2807−2815

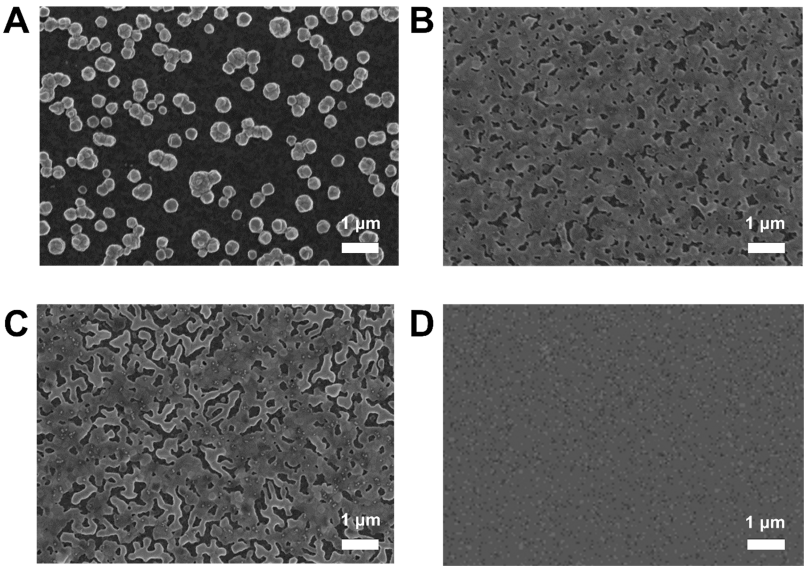

Figure 2. SEM images of $CsSnBr_3$ films (A) without additive, (B) with 20 mol% SnF_2, (C) with 30 mol% SnF_2, and (D) with SnF_2 (30 mol %):TPBI co-additives.

antioxidant) to prevent oxidation of $CsSnBr_3$ and improve the morphology of polycrystalline $CsSnBr_3$ films. The co-additive strategy using a second additive (TPBI) reduced the resultant grain size of $CsSnBr_3$ (from ∼130 to ∼60 nm) by inhibiting the growth of $CsSnBr_3$ grains and enabled the use of a high molar proportion (30 mol%) of SnF_2 additive without causing film non-uniformity. Also, TPBI passivated the $CsSnBr_3$ emission layer, upshifted its valence band maximum (VBM), and thereby improved the EL efficiency and luminance of $CsSnBr_3$ PeLEDs. In sum, we fabricated bright, lead-free inorganic PeLEDs (L = 160 cd m^{-2}) by solution processing; the $CsSnBr_3$ PeLED showed a long device operational lifetime of ∼30 h at 58 cd m^{-2}, which is much longer than the device lifetime of previously reported high-efficiency, lead-free PeLEDs.[36] So far, most reported Sn-based PeLEDs have used 2D perovskite structures.[26,36] Our work improves the understanding of the crystallization kinetics of 3D Polycrystalline $CsSnBr_3$ and provides a simple way to fabricate uniform, solution-processed $CsSnBr_3$ films for bright and stable $CsSnBr_3$ PeLEDs.

To understand the crystallization behavior of $CsSnBr_3$ films, we fabricated three different $CsSnBr_3$ films, (1) without additives, (2) with SnF_2 additive, and (3) with SnF_2:TPBI co-additive, and compared their film morphologies. The additives modified the nucleation and growth processes of the $CsSnBr_3$ films (Figure 1A). One-step spin-coating of inorganic MHPs without additives tends to produce non-uniform polycrystalline film morphologies (Figure 1A, top right) due to the low solubility of the cesium bromide (CsBr) in commonly used organic solvents.[37,38] Addition of SnF_2 to the $CsSnBr_3$ precursor solution yielded improvements in the film morphology of $CsSnBr_3$. SnF_2 molecules can act as heterogeneous nucleation sites,[32] so the use of SnF_2 is expected to increase the number of nucleation sites, and the resultant $CsSnBr_3$ films would have more-uniform surface coverage with a decreased grain size compared to $CsSnBr_3$ films without SnF_2 additive (Figure 1A, middle right). However, addition of excess SnF_2 (i.e., >20 mol %) showed a tendency to form $CsSnBr_3$ aggregates in the films.[32] TPBI functioned as a grain-growth inhibitor for $CsSnBr_3$ films (Figure 1A, bottom right). Also, the use of the SnF_2:TPBI co-additive enabled an increase in the molar percent of SnF_2 additives without causing aggregation of $CsSnBr_3$, which has been a major drawback of using SnF_2 additives. We also suggest a hypothesis on the crystallization processes of $CsSnBr_3$ with additive engineering based on LaMer's nucleation theory[39] and experimental observations on crystallization time (Figure 1B and Table S1). In LaMer's nucleation theory, nucleation occurs only above a certain threshold concentration of precursors (denoted as C_{min}^{nu} in Figure 1B), and growth continues until the precursor concentration reaches an equilibrium value (denoted as C_S in Figure 1B).[39] With SnF_2 additive, the crystallization process is slowed down and the maximum precursor concentration increased, resulting in larger area of the curve (red curve) above C_{min}^{nu} (Figure 1B); this leads to a larger number of nucleation sites than in the control (without additive, black curve). With SnF_2 and TPBI co-additives, the crystallization process is further slowed down, while crystal growth is inhibited by TPBI (blue curve), yielding the highest number of nucleation sites among the three cases. This hypothesis can be supported by experimental observations on the crystallization time (Figure S1 and Table S1). We measured the crystallization time of $CsSnBr_3$ during spin-coating (Table S1) and slow solvent evaporation of $CsSnBr_3$ precursor solutions (Figure S1). In both cases, the co-additive sample showed the slowest crystallization time, verifying our hypothesis. As the number of nucleation sites increased, uniform polycrystalline $CsSnBr_3$ films that have grains much smaller than those of the pristine films (i.e., without additive) were obtained concomitantly. Furthermore, we measured steady-state PL of $CsSnBr_3$ films with and without additives at different stages (stage 1, spin-coating at 3000 rpm for 40 s; stage 2, spin-coating at 3000 rpm for 70 s; stage 3, after solvent drying; stage 4, after annealing at 170 °C for 10 min) (Figure S2). Note that crystallization occurs at ∼40 s for $CsSnBr_3$ without additive, whereas $CsSnBr_3$ with additives forms an adduct phase at ∼40 s (Figure S2B). For the SnF_2 additive, the PL intensity increases with the stage, indicating that crystallization occurs gradually as the film-forming process proceeds (Figure S2C). For the SnF_2:TPBI additive, crystallization of $CsSnBr_3$ occurs at the annealing step, as proven by the dramatic increase in PL intensity at stage 4 (Figure S2C). This observation is in accordance with our hypothesis on the

https://doi.org/10.1021/acsenergylett.2c01010
ACS Energy Lett. 2022, 7, 2807−2815

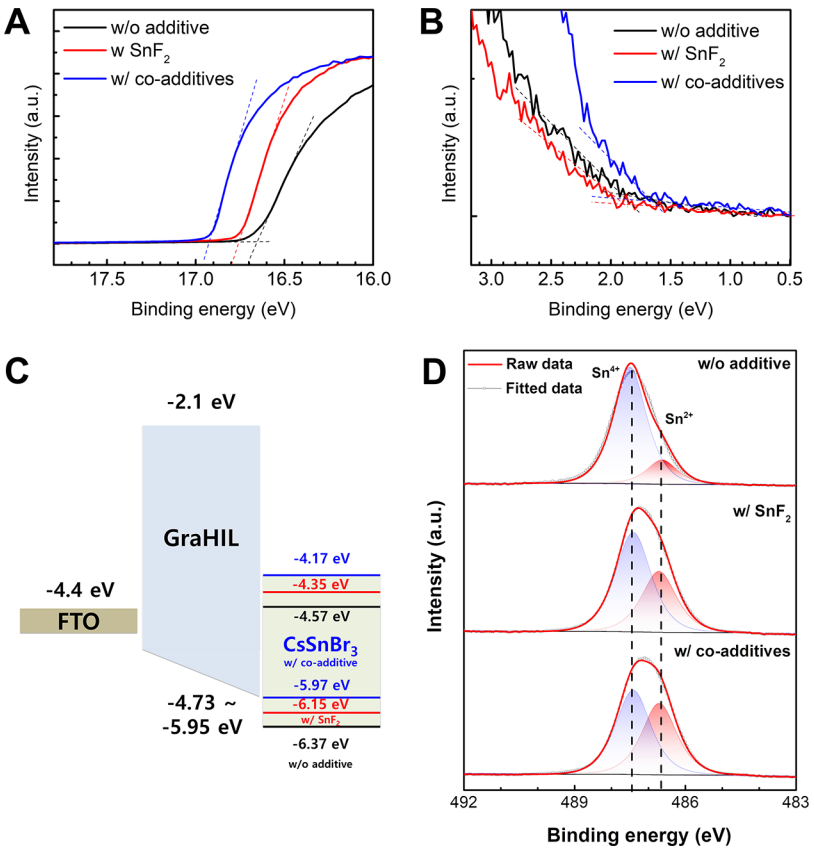

Figure 3. UPS spectra of $CsSnBr_3$ films with SnF_2 additive or SnF_2:TPBI co-additives showing (A) secondary cutoff and (B) VBM. (C) Energy band diagram showing upshift of VBM by co-additive. (D) Deconvolution of XPS Sn 3d spectra of $CsSnBr_3$ films with different additives. The blue and red deconvoluted spectra correspond to Sn^{4+} and Sn^{2+}, respectively.

crystallization behavior of $CsSnBr_3$ with additives (Figure 1). In addition, we have tried to use other electron-transporting small-molecule additives, but the TPBI additive resulted in the best film morphology and PeLED characteristics (Figures S3−S5).

We investigated the surface morphology of polycrystalline $CsSnBr_3$ films obtained using one of the three crystallization processes (Figure 2). Pristine $CsSnBr_3$ film (without additives) showed a non-uniform film morphology with isolated grains (Figure 2A). $CsSnBr_3$ films with SnF_2 additive showed uniform surface coverage, which can probably be attributed to the increase in the number of nucleation sites and suppressed oxidation of Sn^{2+} (Figure 2B and Figure S6).[32] However, addition of >20 mol% SnF_2 caused formation of aggregates of $CsSnBr_3$ on the film, possibly as a result of an excessive number of SnF_2 nucleation sites (Figure 2C and Figure S6).[40] $CsSnBr_3$ films with TPBI and 30 mol% SnF_2 were very dense and uniform with full coverage (Figure 2d); evidently, the TPBI additive prevented the emergence of $CsSnBr_3$ aggregates and improved the surface morphology of the $CsSnBr_3$ film, because TPBI acts as a nucleation inhibitor. In contrast, the surface coverage of $CsSnBr_3$ films with only TPBI additive and no SnF_2 was very poor because of the insufficient density of nucleation sites (Figure S7). Also, we calculated the grain size of two different $CsSnBr_3$ films (i.e., with SnF_2 additive vs with SnF_2:TPBI co-additive). The grain size of the $CsSnBr_3$ film with only SnF_2 additive was 125 nm, but it decreased to 52 nm with the use of SnF_2:TPBI co-additive, which can facilitate the spatial confinement of charge carriers in the nanograins (Figure S8).[7]

X-ray diffraction patterns of $CsSnBr_3$ films were measured to investigate the changes in the crystal structure with varying additives. Three different perovskite films showed a $Pm\bar{3}m$ cubic phase, regardless of the type of additives, and did not show any peak shifts (Figure S9), indicating that the lattice constant was not changed by the additives. The crystallite size was calculated by using the Scherrer equation (36.8 nm with SnF_2 additive, 27.3 nm with SnF_2:TPBI co-additive), leading to the same tendency as observed with the grain size as obtained from the SEM images (Figure S8).

The energy levels of $CsSnBr_3$ films with different additives were determined by performing ultraviolet photoelectron spectroscopy (UPS) (Figure 3A,B). The SnF_2:TPBI co-additive lowered the VBM from 6.37 to 5.97 eV (Figure 3C and Table S2); this effect is presumably due to the incorporation of TPBI.[41] This upshift in VBM of $CsSnBr_3$ emission layers (EMLs) can facilitate hole injection to the EML and suppress unwanted hole injection into the electron transport layer (i.e., TPBI).

X-ray photoelectron spectroscopy (XPS) revealed how SnF_2:TPBI co-additive decreased the self-oxidation behavior of Sn^{2+} (Figure 3D and Figure S10). All XPS spectra had peaks at ~487 eV (= Sn $3d_{5/2}$) and ~496 eV (= Sn $3d_{3/2}$). Addition of SnF_2 caused a downshift of the XPS spectrum compared to that of pristine $CsSnBr_3$; this change clearly shows the prevention of Sn^{2+} oxidation to Sn^{4+}, because Sn^{2+} has lower binding energy than Sn^{4+}. The chemical bonding status of the $CsSnBr_3$ films was analyzed in detail by deconvoluting Sn $3d_{5/2}$ XPS peaks (Figure 3D). The deconvolution yielded two peaks at 486.6 and 487.4 eV, which correspond to Sn^{2+} and Sn^{4+}, respectively.[42] In the pristine $CsSnBr_3$ film, the Sn^{4+} peak was predominant over the Sn^{2+} peak. The incorporation of SnF_2 or SnF_2:TPBI increased

https://doi.org/10.1021/acsenergylett.2c01010
ACS Energy Lett. 2022, 7, 2807−2815

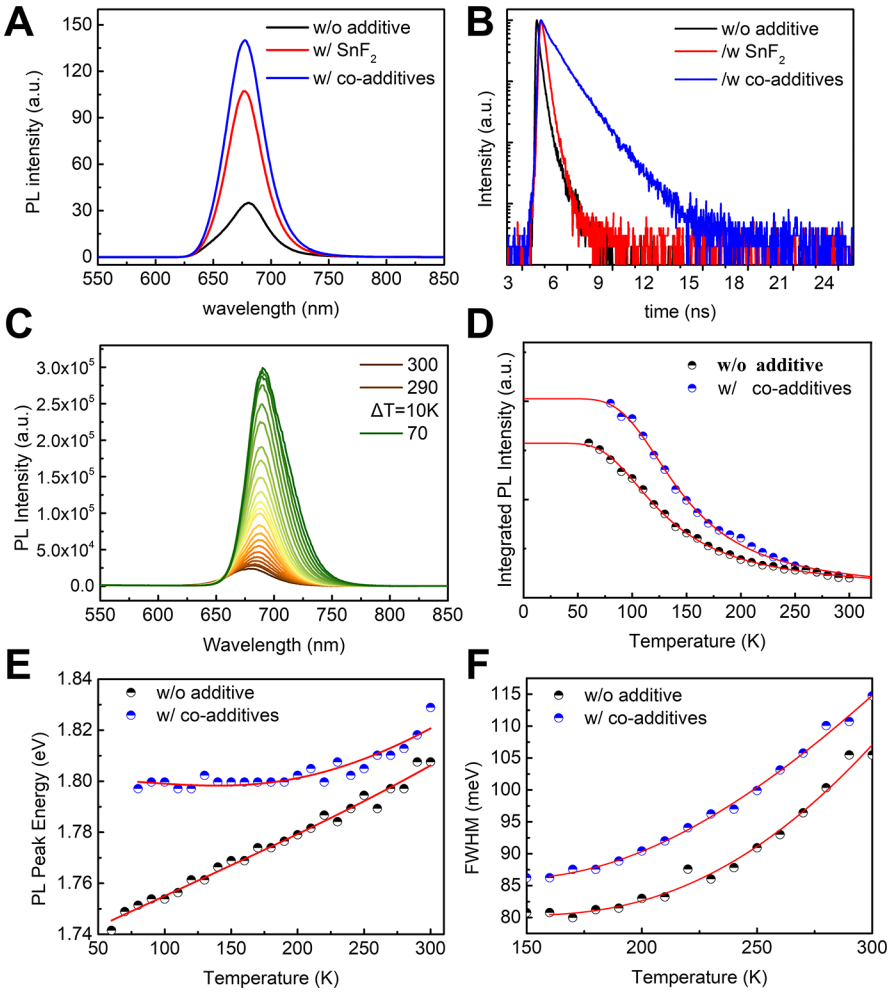

Figure 4. (A) Steady-state PL intensity and (B) PL lifetime of $CsSnBr_3$ films with additive engineering. (C) Temperature-dependent PL spectra of a $CsSnBr_3$ film with SnF_2:TPBI co-additives. (D) PL intensity (integrated from part C) vs temperature, (E) PL peak energy vs temperature, and (F) fwhm vs temperature plots.

the Sn^{2+}/Sn^{4+} ratio from 0.504 to 0.792 (for SnF_2 additive) or 0.902 (for SnF_2:TPBI co-additive), proving that self-oxidation of Sn^{2+} was effectively suppressed by the additives.

To analyze the opto-physical properties of the $CsSnBr_3$ films, we measured the UV−vis absorption, the steady-state spectra, and the time-resolved photoluminescence (PL) spectra (Figure 4). The $CsSnBr_3$ films with additives (i.e., SnF_2 or SnF_2:TPBI) each have a sharp absorption edge around 655 nm, which verifies the formation of uniform $CsSnBr_3$ films with a small roughness (Figure S11A). In contrast, the absorption spectrum of pristine $CsSnBr_3$ film has a high background level due to light scattering caused by the non-uniform film morphology with a high roughness. We determined the band gap of $CsSnBr_3$ (1.77 eV) by using a Tauc plot of the absorption spectrum (Figure S11B). The $CsSnBr_3$ films with SnF_2:TPBI co-additives showed substantially increased steady-state PL intensities and longer PL lifetimes than those of $CsSnBr_3$ films without additives (Figure 4A,B). The PL intensity increased by 5 times, and the average PL lifetime increased from 0.24 to 1.12 ns (Table S3). These changes in PL properties can be attributed to (1) the decreased grain size (Figure 2D) enhancing the radiative recombination by spatial confinement of charge carriers,[7,11] (2) defect passivation at grain boundaries by TPBI,[11] and (3) the prevention of Sn^{4+} formation (Figure 3D and Figure S12A). In correspondence with steady-state PL intensity and PL lifetime results, the PL quantum efficiency (PLQE) of $CsSnBr_3$ films increased from 0.21% to 1.47% with the SnF_2:TPBI co-additive (Table S3). The PL peak position (680 nm) did not differ regardless of the type of additives (Figure S12B). To further investigate the photophysical properties of $CsSnBr_3$ films with our additive engineering strategy, we performed temperature-dependent PL measurements of $CsSnBr_3$ films with SnF_2:TPBI co-additive and without additives (Figure 4C−F, Figure S13, and Tables S4−S6). The measurement was performed from 300 to 60−80 K with steps of 10 K. The fitting results yielded the activation energies (E_a) of the PL quenching process with increasing temperature: E_a = 51.5 meV (for co-additive) and 39.0 meV (for pristine), respectively (Figure 4D) (see Tables S4 for more details about the fitting parameters). Considering the discrepancy between the measured E_a values and previously reported exciton binding energy,[43,44] the main thermal quenching pathway may not be the exciton dissociation. Rather, the PL quenching behavior may be mainly attributed to thermally assisted formation of structural defects and charge carrier traps.[37] For example, a temperature increase can induce halide migration and thus form deep trap states.[45,46] The higher E_a of the co-additive sample than that of the pristine sample implies trap-mediated non-radiative recombination is mitigated in the co-additive sample, which is in line with PLQE and PL lifetime results (Table S3 and Figure 4B). Fitting of the PL peak

https://doi.org/10.1021/acsenergylett.2c01010
ACS Energy Lett. 2022, 7, 2807−2815

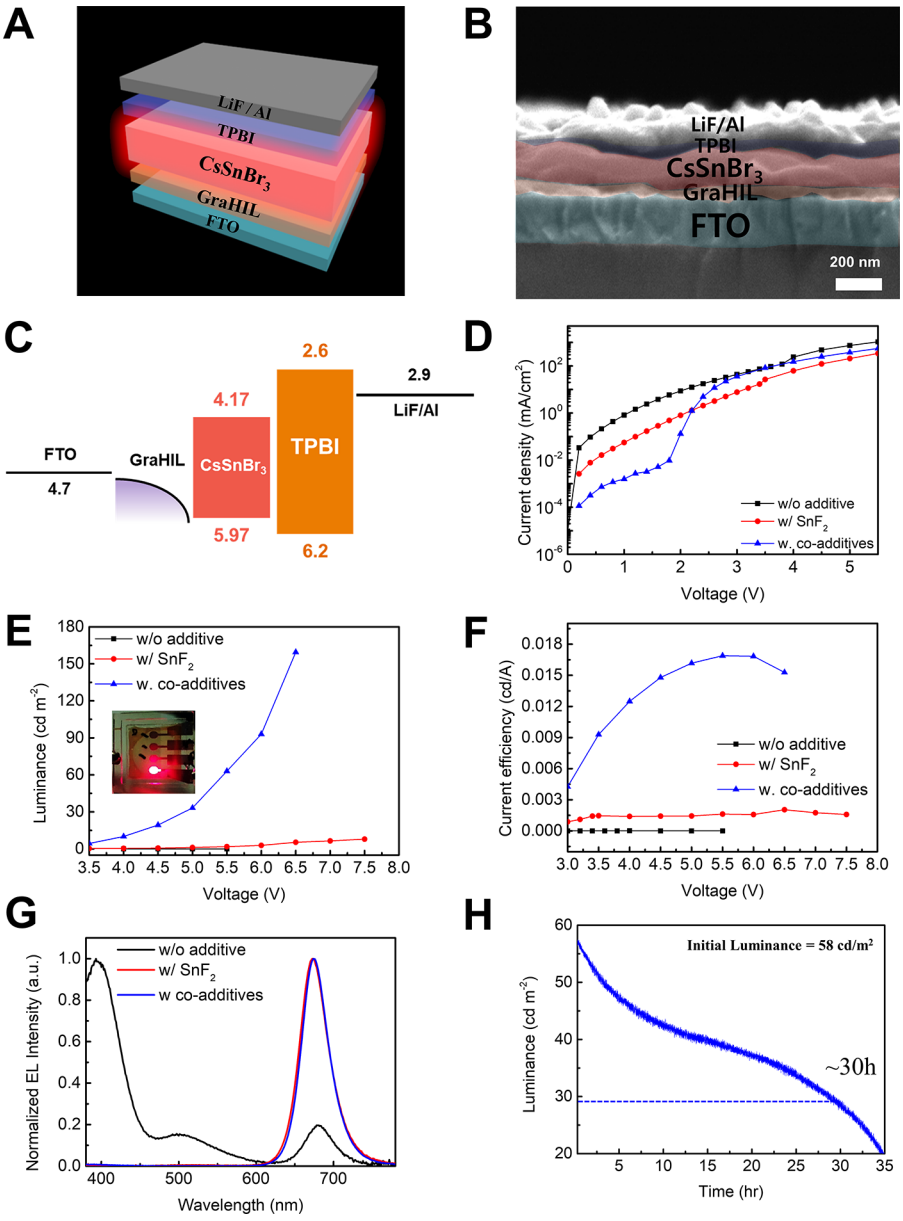

Figure 5. (A) Schematic diagram and (B) cross-section SEM image of the device structure of $CsSnBr_3$ PeLEDs. (C) Energy band diagram of $CsSnBr_3$ PeLEDs. (D) Current density−voltage, (E) luminance−voltage, and (F) current efficiency−voltage characteristics of $CsSnBr_3$ PeLEDs with controlled additive and optimizing ETL thickness. (G) Normalized EL spectra and (H) operational lifetime of $CsSnBr_3$ PeLEDs. Inset of (E): Photograph of a $CsSnBr_3$ PeLED during operation.

energy provides insight on the dependence of the band gap energy on thermal lattice expansion and electron−phonon interaction.[37,47] PL peak energies can be considered as bandgaps and were fitted to[37,47]

$$E_g(T) = E_{g,0} + C_{th}T + C_{ep}\left(\frac{2}{\exp\left(\frac{\hbar\omega}{k_BT}\right) - 1} + 1\right) \quad (1)$$

where E_g (eV) is the bandgap, $E_{g,0}$ (eV) is the un-renormalized bandgap without thermal and phonon contributions, C_{th} (eV/K) is the coefficient regarding thermal expansion, C_{ep} (eV) is the coefficient regarding electron−phonon interaction, and $\hbar\omega$ (eV) is the average optical phonon energy. This equation comes from a one-oscillator model[37,47] and describes the relationship between the thermal expansion of the lattice (second term) and the electron−phonon interaction (third term) to the shift of the bandgap. While the pristine sample showed a linear increase in PL peak energy with temperature for the entire range, the co-additive sample showed an exponential increase in PL peak energy with temperature after ~200 K (Figure 4E and Table S5). This result may imply that the electron−phonon interaction gradually starts to play a role from 200 K in the co-additive sample. It is of interest that the band gap barely changed below 200 K; the physical origin of such behavior requires further studies. In contrast, in the pristine sample, thermal lattice expansion is predominant over electron−phonon interaction for the entire temperature range. That comes from the huge difference of lattice expansion coefficient ($C_{th} = -3.84 \times 10^{-2}$ meV/K (for co-additive) and 0.241 meV/K (for pristine), respectively). Therefore, we can conclude that SnF_2:TPBI co-additive enhanced the influence of the electron−phonon

https://doi.org/10.1021/acsenergylett.2c01010
ACS Energy Lett. 2022, 7, 2807−2815

interaction on the band gap. The fwhm values of temperature-dependent PL spectra were also fitted (Figure 4F and Table S6). The contribution of the exciton−acoustic phonon interaction was negligible, and the changes in fwhm above 160 K were mainly attributable to optical phonon modes, which is in accordance with the literature.[37] As the temperature decreased from 160 K, the fwhm steeply increased for both samples; investigating the physical origin of this behavior is beyond the scope of this study.

To investigate how the additive engineering affects the EL efficiency in the device, we fabricated PeLEDs that had a simple structure of glass substrate/fluorine-doped tin oxide/GraHIL (PFI to PEDOT:PSS = 1:1)[6] (50 nm)/$CsSnBr_3$ (160 nm)/TPBI (30 or 50 nm)/LiF (1 nm)/Al (100 nm) (Figure 5). The PeLED that used pure $CsSnBr_3$ showed almost negligible red emission from $CsSnBr_3$, and the blue emission that comes from the electron transport layer (ETL; TPBI) was rather dominant (Figure 5G). This was ascribed to the poor surface coverage of the $CsSnBr_3$ layer (Figure 2A) and concomitant leakage current passing to the ETL (Figure 5D). The $CsSnBr_3$ PeLED with 20% added SnF_2 showed a clear red emission ($L \approx 8$ cd/m^2, EL peak position = 674 nm) without much leakage current (Figure 5D−F). Improvement of the surface coverage by SnF_2 addition is the most critical factor for the working device. The addition of SnF_2 yields better coverage of $CsSnBr_3$ films and thereby reduces leakage current flowing to the ETL so that recombination occurs in the EML. The PeLED that used the SnF_2:TPBI co-additive was 13 times brighter ($L \approx 107$ cd/m^2) than the PeLED with only added SnF_2 (Figure 5E). The increased luminance and efficiency can be attributed to the increased PLQE of $CsSnBr_3$ layers, improved film morphology, and enhanced hole injection by upshifted VBM. Furthermore, the incorporation of TPBI, an electron-transporting organic small molecule, into the $CsSnBr_3$ layer facilitates electron injection as well because the TPBI is located at the grain boundaries of $CsSnBr_3$ and thereby increases the effective interfacial area between the ETL (TPBI) and $CsSnBr_3$ nanograins.[11] Additionally, we controlled the ETL thickness to further increase the efficiency of PeLEDs (Figure S14). Because Sn-based perovskites have a high hole mobility due to self p-doping,[48] we decreased the ETL thickness from 50 to 30 nm to facilitate electron transport and thus achieve better charge balance in the EML. As a result, the luminance and the current efficiency were significantly increased with this decrease in ETL thickness ($L \approx 160$ cd m^{-2}; CE ≈ 0.016 cd A^{-1}) (Figure 5E,F and Figure S14). To the best of our knowledge, this is the first demonstration of bright (~160 cd m^{-2}), solution-processed, red inorganic, Pb-free PeLEDs. Furthermore, we have measured the stability of the $CsSnBr_3$ PeLEDs; the best device showed a long device lifetime of ~30 h at 58 cd m^{-2} (Figure 5H).

In summary, we developed a simple strategy to fabricate uniform, full-coverage, solution-processed $CsSnBr_3$ films and bright $CsSnBr_3$ PeLEDs without oxidation of Sn^{2+}. The SnF_2 additive functioned as a heterogeneous nucleation site during the crystal growth of $CsSnBr_3$ and thereby improved the surface coverage of $CsSnBr_3$ films without formation of pinholes. Also, SnF_2 addition prevented the spontaneous oxidation of Sn^{2+} to Sn^{4+}, which is a critical obstacle to the use of Sn-based perovskite materials in optoelectronics. Using this method, we achieved lead-free PeLEDs that have $L \approx 8$ cd/m^2 of luminance. Use of SnF_2:TPBI as a co-additive impeded crystal growth during spin-coating of $CsSnBr_3$ precursor solutions; as a result, the grain size of $CsSnBr_3$ was decreased to 52 nm, leading to the high film uniformity and strong spatial confinement of charge carriers within the $CsSnBr_3$ grains. Moreover, TPBI addition significantly increased PLQE of $CsSnBr_3$ films and up-shifted the VBM from 6.37 to 5.97 eV. Finally, we achieved bright and stable $CsSnBr_3$ PeLEDs (maximum luminance of ~160 cd m^{-2} and device lifetime of ~30 h at 58 cd m^{-2}) with SnF_2:TPBI co-additive. This work provides a simple additive strategy to substantially improve the morphology and luminescent properties of $CsSnBr_3$ films for high-brightness and high-stability solution-processed lead-free PeLEDs.

■ ASSOCIATED CONTENT

Supporting Information

The Supporting Information is available free of charge at https://pubs.acs.org/doi/10.1021/acsenergylett.2c01010.

Supplementary methods, preparation and characterization of three different $CsSnBr_3$ films, SEM images of $CsSnBr_3$ depending on ratio of SnF_2 and TPBI, grain-size distribution with $CsSnBr_3$ with SnF_2 and SnF_2:TPBI, X-ray diffraction patterns of $CsSnBr_3$ with different SnF_2 ratios, XPS analysis, and steady-state PL curve of $CsSnBr_3$ films depending on the additives, including Figures S1−S14 and Tables S1−S6 (PDF)

■ AUTHOR INFORMATION

Corresponding Author

Tae-Woo Lee − *Department of Materials Science and Engineering, Seoul National University, Seoul 08826, Republic of Korea; Soft Foundry, Institute of Engineering Research, Research Institute of Advanced Materials, and School of Chemical and Biological Engineering, Seoul National University, Seoul 08826, Republic of Korea;* orcid.org/0000-0002-6449-6725; Email: twlees@snu.ac.kr, taewlees@gmail.com

Authors

Jung-Min Heo − *Department of Materials Science and Engineering, Seoul National University, Seoul 08826, Republic of Korea*

Himchan Cho − *Department of Materials Science and Engineering, Seoul National University, Seoul 08826, Republic of Korea; Department of Materials Science and Engineering, Korea Advanced Institute of Science and Technology (KAIST), Daejeon 34141, Republic of Korea*

Seong-Chul Lee − *PEROLED Inc., Seoul 08826, Republic of Korea; Soft Foundry, Seoul National University, Seoul 08826, Republic of Korea*

Min-Ho Park − *Department of Materials Science and Engineering, Seoul National University, Seoul 08826, Republic of Korea; Institute of Engineering Research, Research Institute of Advanced Materials, Seoul National University, Seoul 08826, Republic of Korea*

Joo Sung Kim − *Department of Materials Science and Engineering, Seoul National University, Seoul 08826, Republic of Korea*

Hobeom Kim − *Department of Materials Science and Engineering, Seoul National University, Seoul 08826, Republic of Korea;* orcid.org/0000-0002-5296-8975

Jinwoo Park − *Department of Materials Science and Engineering, Seoul National University, Seoul 08826, Republic of Korea*

https://doi.org/10.1021/acsenergylett.2c01010
ACS Energy Lett. 2022, 7, 2807−2815

Young-Hoon Kim − *Department of Materials Science and Engineering, Seoul National University, Seoul 08826, Republic of Korea*
Hyung Joong Yun − *Advanced Nano Research Group, Korea Basic Science Institute (KBSI), Daejeon 34133, Republic of Korea*
Eojin Yoon − *Department of Materials Science and Engineering, Seoul National University, Seoul 08826, Republic of Korea*
Dong-Hyeok Kim − *Department of Materials Science and Engineering, Seoul National University, Seoul 08826, Republic of Korea*
Soyeong Ahn − *Department of Materials Science and Engineering, Pohang University of Science and Technology (POSTECH), Pohang, Gyungbuk 790-784, Republic of Korea*
Sung-Joo Kwon − *Department of Materials Science and Engineering, Pohang University of Science and Technology (POSTECH), Pohang, Gyungbuk 790-784, Republic of Korea*
Chan-Yul Park − *Department of Materials Science and Engineering, Seoul National University, Seoul 08826, Republic of Korea*

Complete contact information is available at: https://pubs.acs.org/10.1021/acsenergylett.2c01010

Author Contributions

[#]J.-M.H. and H.C. contributed equally to this work.

Notes

The authors declare no competing financial interest.

■ ACKNOWLEDGMENTS

This work was supported by a National Research Foundation of Korea (NRF) grant funded by the Korea government (Ministry of Science, ICT & Future Planning) (NRF-2016R1A3B1908431).

■ REFERENCES

(1) Quan, L. N.; Rand, B. P.; Friend, R. H.; Mhaisalkar, S. G.; Lee, T. W.; Sargent, E. H. Perovskites for Next-Generation Optical Sources. *Chem. Rev.* **2019**, *119* (12), 7444−7477.
(2) Xing, G.; Wu, B.; Wu, X.; Li, M.; Du, B.; Wei, Q.; Guo, J.; Yeow, E. K. L.; Sum, T. C.; Huang, W. Transcending the Slow Bimolecular Recombination in Lead-Halide Perovskites for Electroluminescence. *Nat. Commun.* **2017**, *8*, 14558.
(3) He, H.; Yu, Q.; Li, H.; Li, J.; Si, J.; Jin, Y.; Wang, N.; Wang, J.; He, J.; Wang, X.; Zhang, Y.; Ye, Z.; et al. Exciton Localization in Solution-Processed Organolead Trihalide Perovskites. *Nat. Commun.* **2016**, *7* (1), 10896.
(4) D'Innocenzo, V.; Grancini, G.; Alcocer, M. J. P.; Kandada, A. R. S.; Stranks, S. D.; Lee, M. M.; Lanzani, G.; Snaith, H. J.; Petrozza, A. Excitons versus Free Charges in Organo-Lead Tri-Halide Perovskites. *Nat. Commun.* **2014**, *5* (1), 3586.
(5) Xiao, Z.; Kerner, R. A.; Zhao, L.; Tran, N. L.; Lee, K. M.; Koh, T. W.; Scholes, G. D.; Rand, B. P. Efficient Perovskite Light-Emitting Diodes Featuring Nanometre-Sized Crystallites. *Nat. Photonics* **2017**, *11* (2), 108−115.
(6) Kim, Y. H.; Cho, H.; Heo, J. H.; Kim, T. S.; Myoung, N. S.; Lee, C. L.; Im, S. H.; Lee, T. W. Multicolored Organic/Inorganic Hybrid Perovskite Light-Emitting Diodes. *Adv. Mater.* **2015**, *27* (7), 1248−1254.
(7) Cho, H.; Jeong, S.-H.; Park, M.-H.; Kim, Y.-H.; Wolf, C.; Lee, C.-L.; Heo, J. H.; Sadhanala, A.; Myoung, N.; Yoo, S.; et al. Overcoming the Electroluminescence Efficiency Limitations of Perovskite Light-Emitting Diodes. *Science.* **2015**, *350*, 1222−1225.
(8) Brenner, T. M.; Egger, D. A.; Kronik, L.; Hodes, G.; Cahen, D. Hybrid Organic—Inorganic Perovskites: Low-Cost Semiconductors with Intriguing Charge-Transport Properties. *Nat. Rev. Mater.* **2016**, *1* (1), 15007.
(9) Tan, Z.-K.; Moghaddam, R. S.; Lai, M. L.; Docampo, P.; Higler, R.; Deschler, F.; Price, M.; Sadhanala, A.; Pazos, L. M.; Credgington, D.; et al. Bright Light-Emitting Diodes Based on Organometal Halide Perovskite. *Nat. Nanotechnol.* **2014**, *9* (9), 687−692.
(10) Hu, H.; Salim, T.; Chen, B.; Lam, Y. M. Molecularly Engineered Organic-Inorganic Hybrid Perovskite with Multiple Quantum Well Structure for Multicolored Light-Emitting Diodes. *Sci. Rep.* **2016**, *6* (1), 33546.
(11) Park, M. H.; Jeong, S. H.; Seo, H. K.; Wolf, C.; Kim, Y. H.; Kim, H.; Byun, J.; Kim, J. S.; Cho, H.; Lee, T. W. Unravelling Additive-Based Nanocrystal Pinning for High Efficiency Organic-Inorganic Halide Perovskite Light-Emitting Diodes. *Nano Energy* **2017**, *42*, 157−165.
(12) Park, M.; Park, J.; Lee, J.; So, H. S.; Kim, H.; Jeong, S.; Han, T.; Wolf, C.; Lee, H.; Yoo, S.; et al. Efficient Perovskite Light-Emitting Diodes Using Polycrystalline Core−Shell-Mimicked Nanograins. *Adv. Funct. Mater.* **2019**, *29* (22), 1902017.
(13) Kim, Y. H.; Wolf, C.; Kim, Y. T.; Cho, H.; Kwon, W.; Do, S.; Sadhanala, A.; Park, C. G.; Rhee, S. W.; Im, S. H.; et al. Highly Efficient Light-Emitting Diodes of Colloidal Metal-Halide Perovskite Nanocrystals beyond Quantum Size. *ACS Nano* **2017**, *11* (7), 6586−6593.
(14) Chiba, T.; Hayashi, Y.; Ebe, H.; Hoshi, K.; Sato, J.; Sato, S.; Pu, Y.-J.; Ohisa, S.; Kido, J. Anion-Exchange Red Perovskite Quantum Dots with Ammonium Iodine Salts for Highly Efficient Light-Emitting Devices. *Nat. Photonics* **2018**, *12* (11), 681−687.
(15) Hailegnaw, B.; Kirmayer, S.; Edri, E.; Hodes, G.; Cahen, D. Rain on Methylammonium Lead Iodide Based Perovskites: Possible Environmental Effects of Perovskite Solar Cells. *J. Phys. Chem. Lett.* **2015**, *6* (9), 1543−1547.
(16) Hao, F.; Stoumpos, C. C.; Cao, D. H.; Chang, R. P. H.; Kanatzidis, M. G. Lead-Free Solid-State Organic-Inorganic Halide Perovskite Solar Cells. *Nat. Photonics* **2014**, *8* (6), 489−494.
(17) Kumar, M. H.; Dharani, S.; Leong, W. L.; Boix, P. P.; Prabhakar, R. R.; Baikie, T.; Shi, C.; Ding, H.; Ramesh, R.; Asta, M.; et al. Lead-Free Halide Perovskite Solar Cells with High Photocurrents Realized through Vacancy Modulation. *Adv. Mater.* **2014**, *26* (41), 7122−7127.
(18) Liao, W.; Zhao, D.; Yu, Y.; Grice, C. R.; Wang, C.; Cimaroli, A. J.; Schulz, P.; Meng, W.; Zhu, K.; Xiong, R.-G.; et al. Lead-Free Inverted Planar Formamidinium Tin Triiodide Perovskite Solar Cells Achieving Power Conversion Efficiencies up to 6.22%. *Adv. Mater.* **2016**, *28* (42), 9333−9340.
(19) Zhao, Z.; Gu, F.; Li, Y.; Sun, W.; Ye, S.; Rao, H.; Liu, Z.; Bian, Z.; Huang, C. Mixed-Organic-Cation Tin Iodide for Lead-Free Perovskite Solar Cells with an Efficiency of 8.12%. *Adv. Sci.* **2017**, *4* (11), 1700204.
(20) Liao, Y.; Liu, H.; Zhou, W.; Yang, D.; Shang, Y.; Shi, Z.; Li, B.; Jiang, X.; Zhang, L.; Quan, L. N.; et al. Highly Oriented Low-Dimensional Tin Halide Perovskites with Enhanced Stability and Photovoltaic Performance. *J. Am. Chem. Soc.* **2017**, *139* (19), 6693−6699.
(21) Wu, C.; Zhang, Q.; Liu, Y.; Luo, W.; Guo, X.; Huang, Z.; Ting, H.; Sun, W.; Zhong, X.; Wei, S.; Wang, S.; Chen, Z.; Xiao, L.; et al. The Dawn of Lead-Free Perovskite Solar Cell: Highly Stable Double Perovskite $Cs_2AgBiBr_6$ Film. *Adv. Sci.* **2018**, *5* (3), 1700759.
(22) Wei, F.; Deng, Z.; Sun, S.; Zhang, F.; Evans, D. M.; Kieslich, G.; Tominaka, S.; Carpenter, M. A.; Zhang, J.; Bristowe, P. D.; et al. Synthesis and Properties of a Lead-Free Hybrid Double Perovskite: $(CH_3NH_3)_2AgBiBr_6$. *Chem. Mater.* **2017**, *29* (3), 1089−1094.
(23) Ma, Z.; Shi, Z.; Yang, D.; Li, Y.; Zhang, F.; Wang, L.; Chen, X.; Wu, D.; Tian, Y.; Zhang, Y.; et al. High Color-Rendering Index and Stable White Light-Emitting Diodes by Assembling Two Broadband Emissive Self-Trapped Excitons. *Adv. Mater.* **2021**, *33* (2), e2001367.
(24) Zhu, Z.; Chueh, C.-C.; Li, N.; Mao, C.; Jen, A. K. Y. Realizing Efficient Lead-Free Formamidinium Tin Triiodide Perovskite Solar Cells via a Sequential Deposition Route. *Adv. Mater.* **2018**, *30* (6), 1703800.
(25) Song, T.-B.; Yokoyama, T.; Stoumpos, C. C.; Logsdon, J.; Cao, D. H.; Wasielewski, M. R.; Aramaki, S.; Kanatzidis, M. G. Importance of

Reducing Vapor Atmosphere in the Fabrication of Tin-Based Perovskite Solar Cells. *J. Am. Chem. Soc.* **2017**, *139* (2), 836−842.
(26) Lanzetta, L.; Marin-Beloqui, J. M.; Sanchez-Molina, I.; Ding, D.; Haque, S. A. Two-Dimensional Organic Tin Halide Perovskites with Tunable Visible Emission and Their Use in Light-Emitting Devices. *ACS Energy Lett.* **2017**, *2* (7), 1662−1668.
(27) Liang, H.; Yuan, F.; Johnston, A.; Gao, C.; Choubisa, H.; Gao, Y.; Wang, Y.; Sagar, L. K.; Sun, B.; Li, P.; et al. High Color Purity Lead-Free Perovskite Light-Emitting Diodes via Sn Stabilization. *Adv. Sci.* **2020**, *7* (8), 1903213.
(28) Hong, W. L.; Huang, Y. C.; Chang, C. Y.; Zhang, Z. C.; Tsai, H. R.; Chang, N. Y.; Chao, Y. C. Efficient Low-Temperature Solution-Processed Lead-Free Perovskite Infrared Light-Emitting Diodes. *Adv. Mater.* **2016**, *28* (36), 8029−8036.
(29) Lu, J.; Guan, X.; Li, Y.; Lin, K.; Feng, W.; Zhao, Y.; Yan, C.; Li, M.; Shen, Y.; Qin, X.; et al. Dendritic $CsSnI_3$ for Efficient and Flexible Near-Infrared Perovskite Light-Emitting Diodes. *Adv. Mater.* **2021**, *33*, 2104414.
(30) Li, B.; Long, R.; Xia, Y.; Mi, Q. All-Inorganic Perovskite $CsSnBr_3$ as a Thermally Stable, Free-Carrier Semiconductor. *Angew. Chemie - Int. Ed.* **2018**, *57* (40), 13154−13158.
(31) Wang, Y.; Zou, R.; Chang, J.; Fu, Z.; Cao, Y.; Zhang, L.; Wei, Y.; Kong, D.; Zou, W.; Wen, K.; et al. Tin-Based Multiple Quantum Well Perovskites for Light-Emitting Diodes with Improved Stability. *J. Phys. Chem. Lett.* **2019**, *10* (3), 453−459.
(32) Xiao, M.; Gu, S.; Zhu, P.; Tang, M.; Zhu, W.; Lin, R.; Chen, C.; Xu, W.; Yu, T.; Zhu, J. Tin-Based Perovskite with Improved Coverage and Crystallinity through Tin-Fluoride-Assisted Heterogeneous Nucleation. *Adv. Opt. Mater.* **2018**, *6* (1), 1700615.
(33) Jokar, E.; Chien, C. H.; Tsai, C. M.; Fathi, A.; Diau, E. W. G. Robust Tin-Based Perovskite Solar Cells with Hybrid Organic Cations to Attain Efficiency Approaching 10%. *Adv. Mater.* **2019**, *31*, 1804835.
(34) Kim, H.; Lee, Y. H.; Lyu, T.; Yoo, J. H.; Park, T.; Oh, J. H. Boosting the Performance and Stability of Quasi-Two-Dimensional Tin-Based Perovskite Solar Cells Using the Formamidinium Thiocyanate Additive. *J. Mater. Chem. A* **2018**, *6* (37), 18173−18182.
(35) Koh, T. M.; Krishnamoorthy, T.; Yantara, N.; Shi, C.; Leong, W. L.; Boix, P. P.; Grimsdale, A. C.; Mhaisalkar, S. G.; Mathews, N. Formamidinium Tin-Based Perovskite with Low Egfor Photovoltaic Applications. *J. Mater. Chem. A* **2015**, *3* (29), 14996−15000.
(36) Yuan, F.; Zheng, X.; Johnston, A.; Wang, Y.; Zhou, C.; Dong, Y.; Chen, B.; Chen, H.; Fan, J. Z.; Sharma, G.; et al. Color-Pure Red Light-Emitting Diodes Based on Two-Dimensional Lead-Free Perovskites. *Sci. Adv.* **2020**, *6* (42), eabb0253.
(37) Cho, H.; Wolf, C.; Kim, J. S.; Yun, H. J.; Bae, J. S.; Kim, H.; Heo, J. M.; Ahn, S.; Lee, T. W. High-Efficiency Solution-Processed Inorganic Metal Halide Perovskite Light-Emitting Diodes. *Adv. Mater.* **2017**, *29*, 1700579.
(38) Ling, Y.; Tian, Y.; Wang, X.; Wang, J. C.; Knox, J. M.; Perez-Orive, F.; Du, Y.; Tan, L.; Hanson, K.; Ma, B.; et al. Enhanced Optical and Electrical Properties of Polymer-Assisted All-Inorganic Perovskites for Light-Emitting Diodes. *Adv. Mater.* **2016**, *28* (40), 8983−8989.
(39) Dabney, M. Y.; Loranz, C. P. *South. Med. J.* **1922**, *15* (3), 242.
(40) Sauter, A.; Roosen-Runge, F.; Zhang, F.; Lotze, G.; Feoktystov, A.; Jacobs, R. M. J.; Schreiber, F. On the Question of Two-Step Nucleation in Protein Crystallization. *Faraday Discuss.* **2015**, *179*, 41−58.
(41) Wu, Z.; Liu, P.; Zhang, W.; Wang, K.; Sun, X. W. Development of InP Quantum Dot-Based Light-Emitting Diodes. *ACS Energy Letters.* **2020**, *5* (4), 1095−1106.
(42) Lee, S. J.; Shin, S. S.; Kim, Y. C.; Kim, D.; Ahn, T. K.; Noh, J. H.; Seo, J.; Il Seok, S. Fabrication of Efficient Formamidinium Tin Iodide Perovskite Solar Cells through SnF_2−Pyrazine Complex. *J. Am. Chem. Soc.* **2016**, *138* (12), 3974−3977.
(43) Huang, L.; Lambrecht, W. R. L. Electronic Band Structure, Phonons, and Exciton Binding Energies of Halide Perovskites $CsSnCl_3$, $CsSnBr_3$, and $CsSnI_3$. *Phys. Rev. B* **2013**, *88* (16), 165203.
(44) Chen, Z.; Yu, C.; Shum, K.; Wang, J. J.; Pfenninger, W.; Vockic, N.; Midgley, J.; Kenney, J. T. Photoluminescence Study of Polycrystalline $CsSnI_3$ Thin Films: Determination of Exciton Binding Energy. *J. Lumin.* **2012**, *132* (2), 345−349.
(45) Cho, H.; Kim, Y. H.; Wolf, C.; Lee, H. D.; Lee, T. W. Improving the Stability of Metal Halide Perovskite Materials and Light-Emitting Diodes. *Adv. Mater.* **2018**, *30* (42), 1704587.
(46) Jin, H.; Debroye, E.; Keshavarz, M.; Scheblykin, I. G.; Roeffaers, M. B. J.; Hofkens, J.; Steele, J. A. It's a Trap! On the Nature of Localised States and Charge Trapping in Lead Halide Perovskites. *Mater. Horizons* **2020**, *7* (2), 397−410.
(47) Wei, K.; Xu, Z.; Chen, R.; Zheng, X.; Cheng, X.; Jiang, T. Temperature-Dependent Excitonic Photoluminescence Excited by Two-Photon Absorption in Perovskite $CsPbBr_3$ Quantum Dots. *Opt. Lett.* **2016**, *41* (16), 3821.
(48) Gupta, S.; Bendikov, T.; Hodes, G.; Cahen, D. $CsSnBr_3$, A Lead-Free Halide Perovskite for Long-Term Solar Cell Application: Insights on SnF_2 Addition. *ACS Energy Lett.* **2016**, *1* (5), 1028−1033.

https://doi.org/10.1021/acsenergylett.2c01010
ACS Energy Lett. 2022, 7, 2807−2815